

# On a practical implementation of particle methods

Alina Chertock<sup>a,\*</sup>, Alexander Kurganov<sup>b</sup>

<sup>a</sup> Department of Mathematics, North Carolina State University, Raleigh, NC 27695, USA

<sup>b</sup> Mathematics Department, Tulane University, New Orleans, LA 70118, USA

Available online 18 May 2006

## Abstract

This paper is devoted to a practical implementation of deterministic particle methods for solving transport equations with discontinuous coefficients and/or initial data, and related problems. In such methods, the solution is sought in the form of a linear combination of the delta-functions, whose positions and coefficients represent locations and weights of the particles, respectively. The locations and weights of the particles are then evolved in time according to a system of ODEs, obtained from the weak formulation of the transport PDEs.

The major theoretical difficulty in solving the resulting system of ODEs is the lack of smoothness of its right-hand side. While the existence of a generalized solution is guaranteed by the theory of Filippov, the uniqueness can only be obtained via a proper regularization. Another difficulty one may encounter is related to an interpretation of the computed solution, whose point values are to be recovered from its particle distribution. We demonstrate that some of known recovering procedures, suitable for smooth functions, may fail to produce reasonable results in the nonsmooth case, and discuss several successful strategies which may be useful in practice. Different approaches are illustrated in a number of numerical examples, including one- and two-dimensional transport equations and the reactive Euler equations of gas dynamics.

© 2006 IMACS. Published by Elsevier B.V. All rights reserved.

MSC: 65M25; 35F10; 34A36; 76V05; 35L65

Keywords: Linear transport equations with discontinuous coefficients; Deterministic particle method; Method of characteristics; Finite-volume methods; Reactive Euler equations of gas dynamics

## 1. Introduction

We consider the linear transport equation:

$$\varphi_t + \operatorname{div}_{\mathbf{x}}(\mathbf{u}\varphi) = S(\mathbf{x}, t, \varphi), \quad (1)$$

subject to the initial condition:

$$\varphi(\mathbf{x}, t) = \varphi_0(\mathbf{x}). \quad (2)$$

Here,  $\mathbf{u} \in \mathbb{R}^d$  and  $\varphi_0 \in \mathbb{R}$  are functions of  $\mathbf{x} \in \mathbb{R}^d$  and  $t$  (not necessarily smooth), and  $S$  is a (possibly singular point) source term. If the coefficient  $\mathbf{u}$  and the data  $\varphi_0$  and  $S$  are sufficiently smooth, it is easy to prove that the

\* Corresponding author.

E-mail addresses: [chertock@math.ncsu.edu](mailto:chertock@math.ncsu.edu) (A. Chertock), [kurganov@math.tulane.edu](mailto:kurganov@math.tulane.edu) (A. Kurganov).

URLs: [www.math.ncsu.edu/~acherto](http://www.math.ncsu.edu/~acherto), [www.math.tulane.edu/~kurganov](http://www.math.tulane.edu/~kurganov).

initial-value problem (1)–(2) has a unique classical solution. When the transport velocity is possibly discontinuous, various existence–uniqueness–stability theories have evolved with a different definition of a solution and different conditions on the transport velocity (see, e.g., [43,44]). The problem is even more complicated in the case of several space dimensions, where the main difficulty is that generalized flows in the sense of PDE, called transport flows, are not unique and the weak stability of the conservation equation is presently out of reach, see, for example, [11,40,6,5] and the references therein. We also refer the reader to [21], where several numerical schemes for one-dimensional (1-D) transport equations with discontinuous coefficients were studied.

Particle methods have been used for a long time to give a numerical solution of purely convective problems, such as the incompressible Euler equation in fluid mechanics [23,32,33] or the Vlasov equation in plasma physics [19]. In these methods, the solution is sought as a linear combination of Dirac distributions:

$$\varphi_N(\mathbf{x}, t) = \sum_{i=1}^N \alpha_i(t) \delta(\mathbf{x} - \mathbf{x}_i^p(t)), \tag{3}$$

whose positions,  $\{\mathbf{x}_i^p(t)\}$ , and coefficients,  $\{\alpha_i(t)\}$ , represent locations and weights of the particles, respectively. The solution is then found by following the time evolution of the locations and the weights of the particles according to a system of ODEs, obtained by considering a weak formulation of the problem and substituting (3) into (1)–(2). In order to recover a proper approximation of the solution  $\varphi(\mathbf{x}, t)$  at some time  $t > 0$ , one needs to regularize the particle solution  $\varphi_N(\mathbf{x}, t)$ , and hence the performance of the method depends on the quality of the regularization procedures, allowing the recovery of the approximate solution from its particle distribution. In the context of linear transport equations with sufficiently smooth coefficients and initial data, the particle methods have been analyzed in [41]. We also refer the reader to [12] for a general introduction of the particle methods and their numerical analysis and to [9] for the study of the convergence rate of these methods. When a particle method is applied to problems with nonsmooth data, the most challenging part of the overall algorithm is recovering point values of the computed solution from its particle distribution. A commonly used type of the reconstruction is the regularization of a particle solution performed by taking a convolution with a so-called cutoff function, which plays the role of a smooth approximation to a delta-function. This procedure works perfectly fine for smooth functions, but may break down when applied to nonsmooth (discontinuous) solutions: depending on the width of the convolution kernel, one may get either a smeared or an oscillatory approximation, as it is demonstrated in Sections 2 and 3.

In this paper, we consider different algorithms for reconstruction of numerical solutions from particle distributions and, in particular, suggest a strategy, which, in most cases, seems to provide the best solution of the recovery problem. We first use a convolution with a low width cutoff function, which results in an oscillatory approximation of the point values, which are then filtered by the nonlinear filter proposed in [15] for the treatment of solution cell averages. Even though this strategy has worked reasonably well in all the examples (both one- and two-dimensional) we considered, no convergence proof is available.

An alternative recovery approach we use in this paper is based on the concept of a dual solution. It was proposed in [7] in the context of the transport equation that describes propagation of passive pollutant in shallow water. Here, we extend it to treat the equation for the mass fraction of the burnt/unburnt gases in reactive flows. The resulting particle method is similar (and in some cases, is equivalent) to the method of characteristics, and provides one with a set of computed point values rather than a particle distribution of the solution. A similar situation occurs when advection of a scalar quantity in a given incompressible flow field is considered.

We would also like to emphasize the advantage of using particle methods for solving the transport equation (1) with a stiff term  $S$ . Such equations arise in many different applications, but in this paper we are concerned with the 1-D Euler equations that model a time-dependent flow of an inviscid, compressible reactive gas:

$$\begin{pmatrix} \rho \\ \rho u \\ E \end{pmatrix}_t + \begin{pmatrix} \rho u \\ \rho u^2 + p \\ u(E + p) \end{pmatrix}_x = 0, \tag{4}$$

where  $\rho$ ,  $u$ ,  $p$ , and  $E$  are the density, velocity, pressure, and the total energy, respectively. The transport equations for the mass fraction of the unburnt gas  $z$ :

$$(\rho z)_t + (\rho u z)_x = -\frac{1}{\varepsilon} \rho z K(\tau), \tag{5}$$

is coupled with the system (4) through the equations of state (EOS):

$$p = (\gamma - 1) \cdot \left[ E - \frac{\rho u^2}{2} - q_0 \rho z \right], \quad \gamma, q_0 = \text{const}, \quad (6)$$

and the Arrhenius kinetics term [13]:

$$K(\tau) = e^{-\tau_c/\tau}, \quad (7)$$

where  $\tau := p/\rho$  is the temperature and  $\tau_c$  is the ignition temperature.

When  $0 < \varepsilon \ll 1$ , the reaction is fast and the time scale associated with the stiff reaction term is much smaller than that associated with the fluid advection. The main difficulty in solving such equations numerically is obtaining the correct propagation speed of the detonation waves in the case of underresolved computations, that is, when both temporal ( $\Delta t$ ) and spatial ( $\Delta x$ ) grid scales are much larger than  $\varepsilon$ . In such a case, one may want to use an operator splitting (fractional step) method, and to replace the solution of the corresponding reaction ODE:

$$(\rho z)_t = -\frac{1}{\varepsilon} \rho z K(\tau), \quad (8)$$

with the deterministic projection operator. However, as it was first observed in [10], such a deterministic projection method may lead to a spurious weak detonation wave that travels with an unphysical propagation speed of one grid cell per time step. This is a result of numerical dissipation present in shock-capturing methods. To overcome this difficulty, several methods have been proposed (see, e.g., [1–3,24,25,27,38]). In Section 4, we demonstrate that applying low dissipative, mesh-free particle methods to this model results in an accurate computed solution even when a problem with a complicated wave interactions is considered.

## 2. Particle methods for transport equations with discontinuous coefficients

We begin with a brief description of the particle method for the initial-value problem (1)–(2). As it is mentioned in Section 1, the solution is sought as a linear combination of Dirac distributions given by (3). Considering a weak formulation of the problem and substituting (3) into (1)–(2) results in the following system of ODEs for the locations,  $\mathbf{x}_i^p(t)$ , and the weights,  $\alpha_i(t)$ , of the particles:

$$\begin{cases} \frac{d\mathbf{x}_i^p(t)}{dt} = \mathbf{u}(\mathbf{x}_i^p, t), \\ \frac{d\alpha_i(t)}{dt} = \beta_i(t), \end{cases} \quad (9)$$

where  $\beta_i$  reflects the contribution of the source term  $S$  (see, e.g., [41,9]). The initial positions of the particles,  $\mathbf{x}_i^p(0)$ , and their initial weights,  $\alpha_i(0)$ , are chosen to provide a high-order approximation to the initial data (2), that is, to accurately approximate the integral equation

$$\sum_{i=1}^N \alpha_i(0) \psi(\mathbf{x}_i^p(0)) = \int_{\mathbf{x}} \varphi_0(\mathbf{x}) \psi(\mathbf{x}) \, d\mathbf{x}$$

for all  $C_0^1$  test functions  $\psi$ . For example, one may cover the support of  $\varphi_0$  with a mesh consisting of cells  $B_i$ ,  $i = 1, \dots, N$ . Then, placing the particles at  $t = 0$  into the centers of mass of the corresponding cells and using the second-order midpoint quadrature gives the following initial data for the system (9):

$$\mathbf{x}_i^p(0) = \mathbf{x}_i^{\text{CM}}, \quad \alpha_i(0) = |B_i| \varphi_0(\mathbf{x}_i^{\text{CM}}), \quad (10)$$

where  $\mathbf{x}_i^{\text{CM}}$  denotes the center of mass of the corresponding cell  $B_i$ .

Notice that since both  $\mathbf{u}$  and  $S$  may be nonsmooth, the right-hand side (RHS) of (9) may be discontinuous as well. However, as long as it is bounded, the existence of a generalized solution of (9)–(10) is guaranteed by the theory of Filippov [16–18]. The uniqueness of the solution of this initial-value problem for a general  $\mathbf{u} \in L^\infty$  and a possibly singular source is a more delicate problem. However, in most practical applications,  $\mathbf{u}$  is a piecewise smooth function: it may be either given explicitly or obtained from the solution of another system as, for instance, in the case of the

reactive Euler equations, where the velocity  $u$  in the transport equation (5) can be computed from (4) using a finite-volume method (see, e.g., [20,26,37]). In the latter case,  $\mathbf{u}(\mathbf{x}_i^p(t), t)$  in (9) can be replaced with  $\tilde{\mathbf{u}}(\mathbf{x}_i^p(t), t)$ , where  $\tilde{\mathbf{u}}$  is piecewise polynomial interpolant reconstructed from the cell averages of  $\mathbf{u}$ , computed over the fixed computational mesh. Such a piecewise polynomial will be, in general, discontinuous at every cell interface, but, for a fixed mesh,  $\tilde{\mathbf{u}}$  may only be discontinuous along the surfaces of codimension 1, and therefore one can replace  $\tilde{\mathbf{u}}$  with its smooth approximation. This would guarantee uniqueness of the solution of the initial-value problem (9)–(10). In practice, however, no particular smoothing procedure is required: when the problem (9)–(10) is solved numerically, either the left or the right or any intermediate value of  $\mathbf{u}$  at the discontinuity may be used for computing the RHS of (9) if  $(\mathbf{x}_i^p(t), t)$  happens to lie right on the discontinuity surface. As for a numerical treatment of a singular source  $S$ , we would like to refer the reader to a specific approach discussed in [8,7] in the context of propagation of a passive pollutant in shallow water.

At the final time  $t_{\text{fin}}$ , the solution  $\varphi(\mathbf{x}, t_{\text{fin}})$  should be recovered from the computed particle approximation  $\varphi_N(\mathbf{x}, t_{\text{fin}})$ . As it has been mentioned above, a commonly used way of computing point values of the numerical solution is a regularization of (3), which is usually performed by taking a convolution product with a smooth kernel  $\zeta_\varepsilon(x)$ , namely, by approximating

$$\varphi(\mathbf{x}, t_{\text{fin}}) \approx (\varphi * \zeta_\varepsilon)(\mathbf{x}, t_{\text{fin}}) := \sum_{i=1}^N \alpha_i(t_{\text{fin}}) \zeta_\varepsilon(\mathbf{x} - \mathbf{x}_i^p(t_{\text{fin}})), \tag{11}$$

where  $\zeta_\varepsilon$  serves as a smooth approximation of the  $\delta$ -function satisfying

$$\zeta_\varepsilon = \frac{1}{\varepsilon^d} \zeta\left(\frac{\mathbf{x}}{\varepsilon}\right), \quad \varepsilon > 0, \quad \int_{\mathbb{R}^d} \zeta(\mathbf{x}) \, d\mathbf{x} = 1. \tag{12}$$

There is an extensive discussion in the literature on the selection of a cutoff function  $\zeta$  and its relation to the accuracy of particle methods (see, e.g. [12,41] and the references therein). In particular, classical error estimates, obtained in [41] for the linear transport equation with sufficiently smooth coefficients and initial data, show that the error is equal to  $C_1 \varepsilon^k + C_2 (\Delta x / \varepsilon)^m$ , where  $\Delta x$  is a mean interparticle distance,  $m$  is related to the smoothness of  $\zeta$ , and  $k$  is a number of vanishing moments of  $\zeta$ . Since  $C_1$  and  $C_2$  depend on the smoothness of the data [41], this estimate, in general, fails when the coefficients and/or initial data are discontinuous, in which case the above regularization may either smear the discontinuities or lead to oscillations, depending on the value of  $\varepsilon$ . In the following example, we illustrate the failure of the smoothing procedure (11) and propose a way of its improvement. Even though we show the numerical results for this particular example only, the new recovery method can be easily extended to a more general case.

**Example 1.** Consider the 1-D transport equation:

$$\varphi_t + (u(x, t)\varphi)_x = 0, \quad u(x, t) = \begin{cases} \frac{1}{2}(x + 1), & \text{if } -1 < x < 0, \\ \frac{1}{2}, & \text{if } 0 < x < t, \\ 0, & \text{otherwise,} \end{cases} \tag{13}$$

subject to the initial condition

$$\varphi(x, 0) = \begin{cases} 1, & \text{if } -1 < x < 1, \\ 0, & \text{otherwise.} \end{cases} \tag{14}$$

In this case, the weights obviously do not change in time, that is,  $\alpha_i(t) \equiv \alpha_i(0) =: \alpha_i$ , and the system (9) reduces to

$$\frac{d\mathbf{x}_i^p(t)}{dt} = u(\mathbf{x}_i^p, t). \tag{15}$$

The system (15) has been solved numerically by the third-order strong stability preserving (SSP) Runge–Kutta method [22] and at the final time  $t = t_{\text{fin}}$  point values of the computed solution are recovered using formula (11). In all the computations the Gaussian kernel,  $\zeta_\varepsilon(x) = \frac{1}{\sqrt{2\pi}\varepsilon} e^{-x^2/2\varepsilon^2}$ , has been used, but we note that other smooth kernels give similar results.

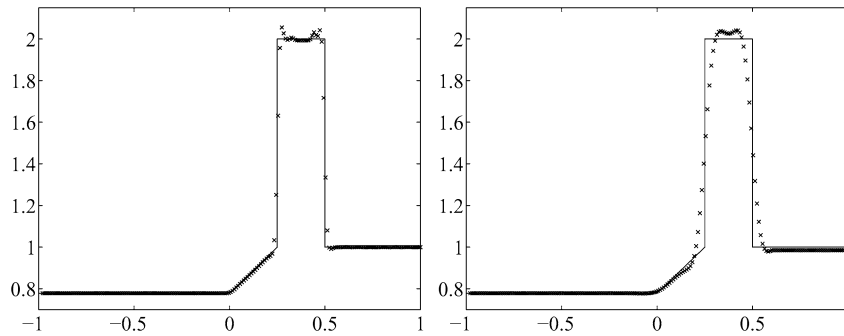


Fig. 1. The solution of (13)–(14) obtained with: (left)  $\varepsilon_i = 0.25\sqrt{\Delta_i^{\max}}$ , (right)  $\varepsilon_i = 0.75\sqrt{\Delta_i^{\max}}$ .

The choice of suitable values of its width parameter  $\varepsilon$  plays now an essential role. Intuitively, it is clear that if  $\varepsilon$  is too small compared to the distances between the particles and their neighbors, the approximate solution defined by (11) will vanish away from the  $\varepsilon$ -neighborhood of the particles and is thus irrelevant. On the other hand, large values of  $\varepsilon$  will generate unacceptable smoothing errors.

It is known (see, e.g. [41]) that for sufficiently smooth solutions,  $\varepsilon \sim \sqrt{\Delta x}$ , where  $\Delta x$  is a mean interparticle distance, usually leads to reliable results. However, since neither the solution of the initial-value problem (13)–(14) nor the coefficient in Eq. (13) is smooth, the ratio between the largest and the smallest distance between neighboring particles may be very large and the mean interparticle distance becomes useless. Therefore, we first of all modify the “standard” convolution procedure (11) by taking kernels of locally varying width, whose size depends on the distance between the particles, that is, we approximate the solution at the final time by

$$\varphi_N^\varepsilon(x, t_{\text{fin}}) = \sum_{i=1}^N \alpha_i \zeta_{\varepsilon_i}(x - x_i^p(t)). \quad (16)$$

Here the smoothing length  $\varepsilon_i$  of each local kernel is selected in a point-wise manner, according to the following formula:

$$\varepsilon_i = C\sqrt{\Delta_i^{\max}}, \quad \Delta_i^{\max} = \max(|x_{i+1} - x_i|, |x_i - x_{i-1}|), \quad (17)$$

and the values of  $C$  depend on  $\Delta_i^{\max}$ .

Numerical solutions of (13)–(14) at time  $t_{\text{fin}} = 0.5$  for the values of  $C = 0.25$  and  $C = 0.75$  are presented in Fig. 1 (the solid line represents the exact solution). One can clearly observe an oscillatory behavior for  $C = 0.25$  in Fig. 1 (left) and a poor resolution of discontinuities for  $C = 0.75$  in Fig. 1 (right). In both cases, the number of initially uniformly distributed particles is  $N = 200$ .

In the case of a smaller  $C$ , however, the oscillation can be removed by applying a nonlinear filter proposed in [15]. To this end, we first compute discrete values  $\{\varphi(x_j, t_{\text{fin}})\}$  of the solution at uniform grid points  $x_j$  and then utilize a filter algorithm similar to Algorithm 2.3 in [15]. Notice, that the nonlinear filter is applied only once, as a post-processing, not after every time step as in [15], and only if oscillations are observed. The “filtered” and the exact solutions of the initial-value problem (13)–(14) are shown in Fig. 2. As one clearly see, the oscillations, caused by the recovering procedure (16) with  $\varepsilon_i = 0.25\sqrt{\Delta_i^{\max}}$ , have been successfully removed by the nonlinear filter.

**Remark.** Another possibility to recover point values of the computed solution from its particle distribution was studied in [8] in the context of modeling the transport of passive pollutant in shallow water. The computed particle data were interpreted as integrals of the approximated solution over some nonoverlapping intervals around the particles (the union of the intervals has to cover the whole computational domain). Then, dividing the weights  $\alpha_i$  by the lengths of the corresponding intervals, the cell averages  $\bar{\varphi}_i$  were obtained. Still, in some cases the resulting piecewise constant approximation were oscillatory and the nonlinear filter from [15] or another filtering procedure should be implemented as a post-processing (see, e.g., the numerical experiments in [7]). Since in the case of more than one space dimension, particles can form a very complicated unstructured grid, a multi-dimensional generalization of this technique is rather problematic, and therefore it is not considered in this paper.

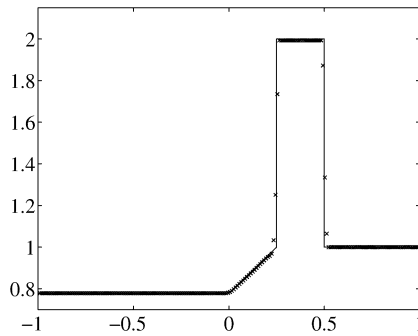


Fig. 2. The solution from Fig. 1 (left) after filtering.

### 3. Advection in incompressible flow

In this section, we consider a special case in which the advection of a scalar concentration or density function  $\varphi(\mathbf{x}, t)$  in a specified velocity field  $\mathbf{u}(\mathbf{x}, t)$  is governed by the conservation law

$$\varphi_t + \text{div}_{\mathbf{x}}(\mathbf{u}\varphi) = 0. \tag{18}$$

We assume that the flow is incompressible, so that

$$\text{div}_{\mathbf{x}} \mathbf{u} = 0 \tag{19}$$

everywhere and Eq. (18) can be written equivalently as a variable coefficient advection equation

$$\varphi_t + \mathbf{u} \cdot \nabla_{\mathbf{x}} \varphi = 0. \tag{20}$$

In this case, the particle method is equivalent to the method of characteristic and provides one with a set of computed point values rather than a particle distribution of the solution. Indeed, the particle trajectories for Eq. (18), determined by (9), coincide with the characteristic curves for Eq. (20), and thus the corresponding point values of the solution at the final time  $t = t_{\text{fin}}$  are

$$\varphi(\mathbf{x}_i^p(t_{\text{fin}}), t_{\text{fin}}) = \varphi(\mathbf{x}_i^p(0), 0). \tag{21}$$

Solving Eq. (18) or (20) numerically is a rather challenging task. A number of (conservative and nonconservative) high-resolution advection algorithms have been developed in recent years (see, e.g., [14,34,37] and the references therein). Methods based on the advection form (20) are sometimes more successful than the conservative schemes [34], but can often cause nonconservative behavior and a change in the total mass that is unacceptable in many applications. Conservative high-resolution algorithms for (18) may, on the other hand, lead to oscillations and loss of positivity [14,34], and, as a result, to physically irrelevant (and unstable) solutions. A great feature of the particle method is that it combines the advantages of the built-in conservation (since the weights do not change in time) and positivity preserving property (due to the characteristics interpretation (21)). As an example we consider a two-dimensional (2-D) problem taken from [34], which has also been considered in [14].

**Example 2.** We solve a 2-D test problem in which a passive tracer is advected in a nondivergent deformational flow according to the equation

$$\varphi_t + (u\varphi)_x + (v\varphi)_y = 0, \quad (x, y) \in [0, 1] \times [0, 1]. \tag{22}$$

The initial concentration of the tracer is given by

$$\varphi(x, y, 0) = \frac{1 + \cos(\pi r)}{2}, \quad r(x, y) = \min\left(1, 4\sqrt{\left(x - \frac{1}{4}\right)^2 + \left(y - \frac{1}{4}\right)^2}\right). \tag{23}$$

The velocity field is a swirling shear flow defined as follows:

$$\begin{cases} u(x, y) = \sin^2(\pi x) \sin(2\pi y) \cos(\pi t/5), \\ v(x, y) = -\sin^2(\pi y) \sin(2\pi x) \cos(\pi t/5), \end{cases} \tag{24}$$

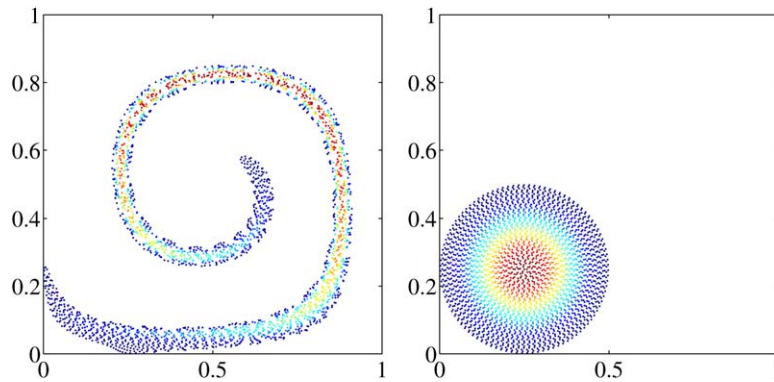


Fig. 3. Locations of particles at time  $t = 2.5$  (left) and  $t = 5$  (right).  $N = 2500$ .

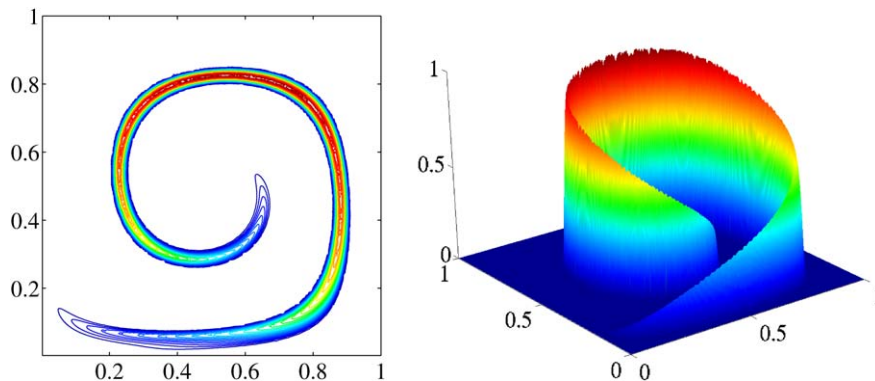


Fig. 4. The characteristics solution of (22)–(24) at  $t = 2.5$ , recovered using the bilinear-linear procedure—contour (left) and surface (right) plots.  $N = 10000$ .

and satisfies  $u = v = 0$  on the boundaries. The flow slows down and reverses direction in such a way that every fluid parcel returns to its original position after five time units, so that the correct tracer distribution at  $t = 5$  should be identical to the initial field. This gives a very useful test problem since we know the true solution at time  $t_{\text{fin}} = 5$  even though the flow field has a quite complicated structure.

We start by uniformly distributing particles inside the support of  $\varphi$  at time  $t = 0$ , and let them evolve according to (9), which is solved numerically using the explicit large stability domain Runge–Kutta ODE solver [35,36]. Locations of  $N = 2500$  particles at  $t_{\text{fin}} = 2.5$  and  $t_{\text{fin}} = 5$ , are shown in Fig. 3. As one may clearly see, the particle distribution at time  $t_{\text{fin}} = 5$  is almost uniform, while this is not the case for the intermediate stage of evolution,  $t_{\text{fin}} = 2.5$ , where certain gaps between the particles are observed. Appearance of these gaps makes it difficult to recover point values of the computed solution at the points  $(x, y) \neq (x_i^P(t_{\text{fin}}), y_i^P(t_{\text{fin}}))$ .

We first assume that the point values at  $(x_i^P(t_{\text{fin}}), y_i^P(t_{\text{fin}}))$  are given by (21). Then, the values at the points inside the spiral-like structure, formed at time  $t_{\text{fin}} = 2.5$ , are obtained with the help of a bilinear interpolation, while the values at the points near the spiral boundary are computed by the corresponding “one-sided” linear extrapolation. Such a bilinear-linear recovery procedure results in a reasonable approximate solution, especially when the number of particles is relatively large, see Fig. 4. Obviously, a more sophisticated interpolation-extrapolation technique may be used, though it is clear that when gaps between particles are developed, a certain part of the solution cannot be accurately captured. An alternative approach is to recover the point values of the computed solution with the help of the convolution with the Gaussian kernel of an appropriate (!) width followed by the filtering (the nonlinear filter from [15] is now applied in a dimension-by-dimension manner). This also leads to a reasonable solution though appearance of an artificial spike-like structure in the middle of the spiral significantly affects the quality of the resolution, see Fig. 5.

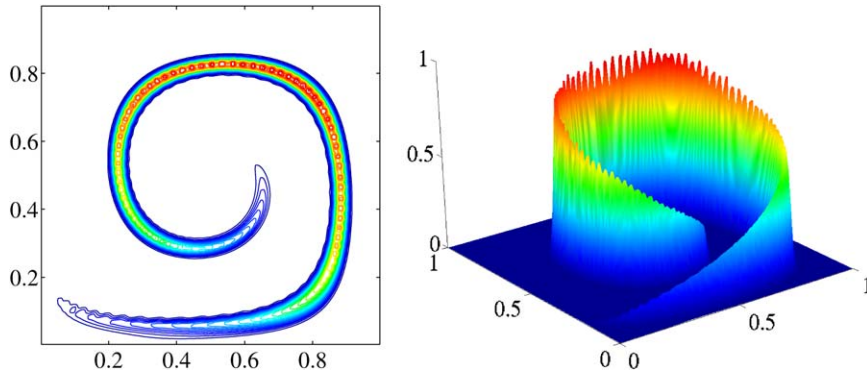


Fig. 5. The particle solution of (22)–(24) at  $t = 2.5$ , recovered using the convolution with the Gaussian with constant  $\varepsilon = 1.5\sqrt{\Delta}$  followed by the filtering—contour (left) and surface (right) plots.  $N = 10000$ ,  $\Delta$  is an initial mean interparticle distance.

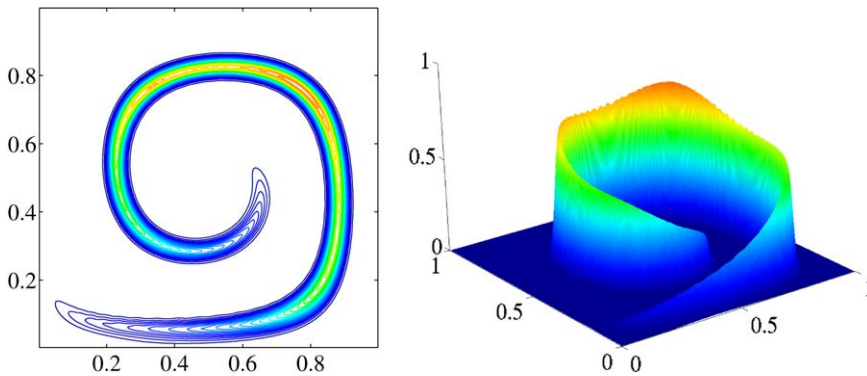


Fig. 6. The same as Fig. 5 but with  $\varepsilon = 2.5\sqrt{\Delta}$ .

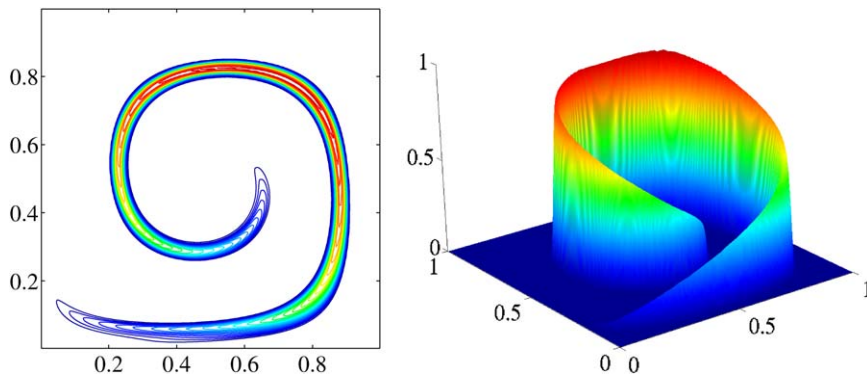


Fig. 7. The finite-volume solution of (22)–(24) at  $t = 2.5$  computed by the semi-discrete second-order upwind scheme on the  $226 \times 226$  uniform mesh—contour (left) and surface (right) plots.

Obviously, one may take larger  $\varepsilon_i$ , but then the resulting solution gets much more diffusive (Fig. 6), and the main advantage of low dissipative particle methods is completely lost.

It is instructive to compare the results obtained by the characteristics/particle method with the solution computed by an alternative, say, finite-volume method. For fair comparison, we take the uniform  $113 \times 113$  and  $226 \times 226$  meshes, which provide the same resolution of the initial pulse as its initial particle approximations with 2500 and 10000 particles, respectively. In Fig. 7, we show the solution of the problem (22)–(24) at  $t_{\text{fin}} = 2.5$ , computed by the

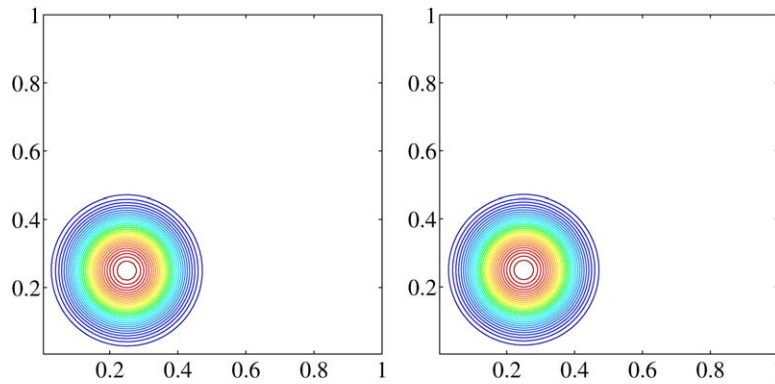


Fig. 8. The characteristics solutions of (22)–(24) at  $t = 5$ , computed with  $N = 2500$  (left) and  $N = 10000$  (right) particles and recovered using the bilinear-linear procedure.

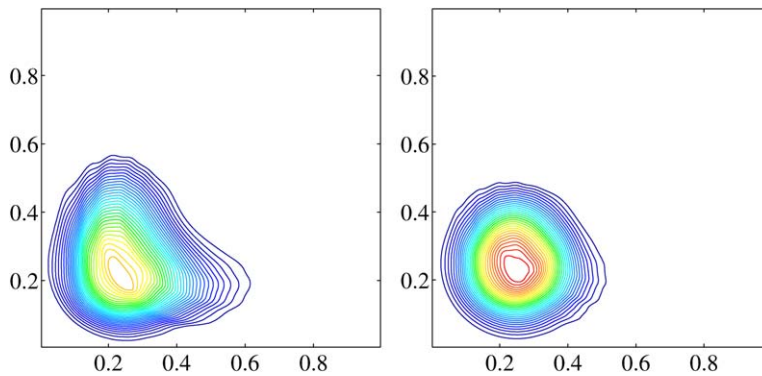


Fig. 9. The finite-volume solutions of (22)–(24) at  $t = 5$  computed by the semi-discrete second-order upwind scheme on a on the  $113 \times 113$  (left) and  $226 \times 226$  (right) uniform meshes.

Table 1  
CPU times required to compute the solution at time  $t = 5$

Second-order upwind scheme		Particle method	
Number of cells	CPU time	Number of particles	CPU time
$56 \times 56$	7.12	625	0.69
$113 \times 113$	64.51	2500	3.14
$226 \times 226$	512.0	10000	19.1

Notice that in order to perform a fair comparison of the methods, the number of cells (left column) and the number of particles (right column) are taken to be different due to the nonuniform initial distribution of particles.

positivity-preserving semi-discrete second-order upwind scheme (a spatial piecewise linear reconstruction is obtained using the generalized MinMod2 limiter [31,42,39] and the time discretization is performed using the third-order SSP Runge–Kutta method [22]). This solution is nonoscillatory but a little more diffusive than the one in Fig. 4. The main advantage of the particle/characteristics method is, however, its much better shape-preserving property. In order to clearly demonstrate this, we compare the characteristics and finite-volume solutions at a larger time  $t_{\text{fin}} = 5$ : the characteristics solutions with 2500 and 10 000 particles, shown in Fig. 8, are much more accurate than their finite-volume counterparts, presented in Fig. 9. Another advantage of the particle method is its self adaptivity (due to the mesh-free nature) and computational efficiency. To demonstrate the latter, we compare the CPU times required to obtain the solution by both the second-order upwind scheme and the particle method at time  $t_{\text{fin}} = 5$ , see Table 1. The CPU times were measured on a Power Mac G4 1.25 GHz processor.

#### 4. Hybrid finite-volume-particle method for stiff detonation waves

We consider the 1-D reactive Euler equations (4)–(7) with a very fast reaction rate ( $\varepsilon \ll 1$ ). We are interested in developing underresolved ( $\Delta t \gg \varepsilon$ ,  $\Delta x \gg \varepsilon$ ) numerical methods that are capable to accurately capture the main wave structure of the solution without resolving the small scale detonation waves. As it was mentioned in Section 1, an operator splitting, followed by the deterministic projection method for the fast reaction ODE (8), typically results in appearance of weak detonation waves propagating with an unphysical speed, proportional to the spatial mesh size. This is caused by a numerical dissipation, which artificially smears discontinuities present in the mass fraction of the unburnt gas  $z$ . Several strategies have been proposed as a remedy to this problem [1–3,24,25,27,38]. Here, we propose a new method, which may become a simple, robust and reliable alternative to the existing methods.

Our main idea is to solve the system (4) by a finite-volume method, while applying a particle method to the stiff transport equation (5). By doing so, we take an advantage of the low dissipation and the mesh-free feature of the particle method: the only smearing will be caused by the recovery procedure, which will be performed in a special way that ensures that no artificially fast or slow reaction will be triggered. The resulting hybrid finite-volume-particle (FVP) method is the method we have developed in [8,7] for the models of propagation of passive pollutant in shallow water.

Our particular choice of the finite-volume method is the semi-discrete second-order central-upwind scheme from [28], which is a recent low dissipative modification of the central-upwind schemes introduced in [30,29]. We use the central-upwind scheme with the generalized MinMod $\theta$  piecewise linear reconstruction [31,42,39] with  $\theta = 1.3$  and the third-order SSP Runge–Kutta ODE solver from [22]. Since the system (4) can be solved independently of the transport equation (5), the aforementioned particle method (9) with  $\varphi := \rho z$  and  $S := -\frac{1}{\varepsilon} \rho z K(\tau)$  can be applied directly to (5). In this case,  $\beta_i = -\frac{1}{\varepsilon} K(\tau) \alpha_i$  and the velocities  $u(x_i^P(t), t)$  can be calculated from the piecewise linear reconstruction of  $\rho u$  and  $\rho$ , used for solving (4) by the central-upwind scheme. After applying the particle method to Eq. (5), the point values of  $\rho z$  can be, in principle, recovered using (11). However, since  $\rho z$  should be used in the EOS (6), it has to be recovered at every time step, and the smearing caused by doing so may trigger a reaction of a wrong rate.

Therefore, we use the method, proposed in [7], that allows to completely avoid any loss of resolution attributed to the regularization of the particle distribution. The idea is to consider an equation for  $z$ ,

$$z_t + uz_x = -\frac{1}{\varepsilon} K(\tau)z, \tag{25}$$

which is equivalent to Eq. (5) for smooth solutions, and, at the same time, is dual to it. Then, multiplying (5) by  $z$  and (25) by  $\rho z$ , adding them up, and integrating with respect to  $x$ , we obtain

$$\frac{d}{dt} \int_R (\rho z)z \, dx = - \int_R \frac{2}{\varepsilon} K(\tau)(\rho z)z \, dx, \tag{26}$$

provided either  $z$  or  $u$  vanish at infinity. Let us now take  $(\rho z)(x, 0)$  to be a single particle,  $\alpha_i(0)\delta(x - x_i^P(0))$ , which, as it is explained above, will evolve in time according to the ODE system (9). Then Eq. (26) reduces to the single ODE along the generalized characteristics  $x_i^P(t)$ :

$$\frac{d}{dt} [(\alpha z)(x_i(t), t)] = -\frac{2}{\varepsilon} K(\tau)(\alpha z)(x_i^P(t), t), \tag{27}$$

which is solved in combination with (9). Finally, the point values of  $z$  are obtained by

$$z(x_i^P(t), t) = \frac{(\alpha z)(x_i^P(t), t)}{\alpha_i(t)}.$$

As we will illustrate below (see Figs. 10–12), this usually results in a very sharp resolution of the interfaces in  $z$ . However, the obtained point values of  $z$  are only available at  $x = x_i^P(t)$ , and in order to be able to use the EOS (6) at  $x \neq x_i^P(t)$ , the values of  $z$  there has to be interpolated. In our numerical experiments, we have used the simplest linear spline interpolation, which is good enough since typical  $z$  is a piecewise constant function. Notice that almost every interpolation will introduce some intermediate values, which will be, in fact, projected to either  $z = 0$  or  $z = 1$

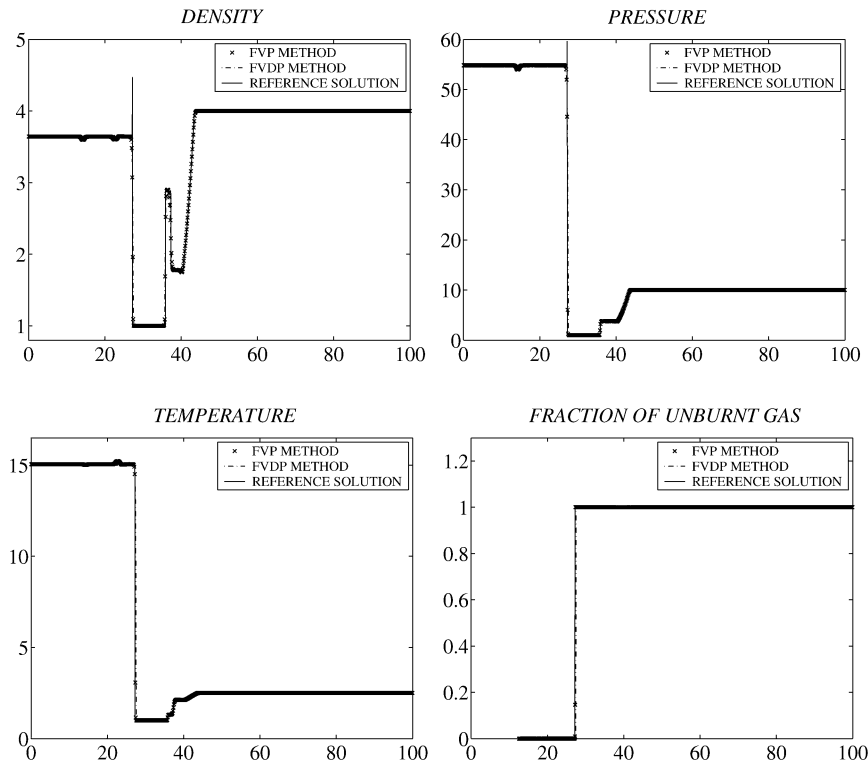


Fig. 10. Solutions of (4)–(5), (28)–(29) computed by both the FVP and FVDP methods at  $t = 2$ .

(provided  $\varepsilon$  is small), but since  $\{x_i^p(t)\}$  is not mesh-oriented for  $t > 0$ , this will not lead to a wrong reaction speed proportional to  $\Delta x$ .

We demonstrate the performance of the proposed FVP method by applying it in a rather complicated situation, where a detonation wave collides with a shock, a contact discontinuity, and a rarefaction wave. This example is taken from [25,2]. The parameters are:

$$\gamma = 1.2, \quad q_0 = 50, \quad \tau_c = 3, \quad \frac{1}{\varepsilon} = 230.75. \quad (28)$$

The initial data are:

$$(\rho, u, p, z)(x, 0) = \begin{cases} (\rho_l, u_l, p_l, 0), & \text{if } x \leq 10, \\ (\rho_m, u_m, p_m, 1), & \text{if } 10 < x \leq 40, \\ (\rho_r, u_r, p_r, 1), & \text{if } x > 40, \end{cases} \quad (29)$$

where  $\rho_l = 3.64282$ ,  $u_l = 6.2489$ ,  $p_l = 54.8244$ ;  $\rho_m = 1$ ,  $u_m = 0$ ,  $p_m = 1$ ; and  $\rho_r = 4$ ,  $u_r = 0$ ,  $p_r = 10$ . These data correspond to a right moving detonation, a left moving shock, a stationary contact, and a right moving rarefaction. A series of collisions occur after the detonation catches up with the other waves.

We compare the solutions, computed by the FVP method and by the “finite-volume deterministic projection” (FVDP) method, which is obtained by applying the semi-discrete second-order central-upwind scheme to the system (4)–(5) using the operator splitting and the deterministic projection method for solving the reaction ODE (8). We take both the initial distance between the uniformly distributed particles and the uniform mesh size  $\Delta x = 0.125$ , and  $\Delta t = 0.05$ . The reference solution is computed using the fully resolved calculation with  $\Delta x = 0.005$  and  $\Delta t = 0.00025$ .

In Fig. 10, we show the computed solutions (density, pressure, temperature, and fraction of unburnt gas) at time  $t = 2$  (before collisions). At this time, both methods provide rather accurate approximations. The results at the later time  $t = 4$  (after the collision with the shock, but before the collision with the rarefaction wave) are shown in Fig. 11. At this time, only the density is sufficiently accurately captured by the FVDP method, while an unphysical weak detonation wave has already appeared in the other components. At the same time, the location and amplitude of

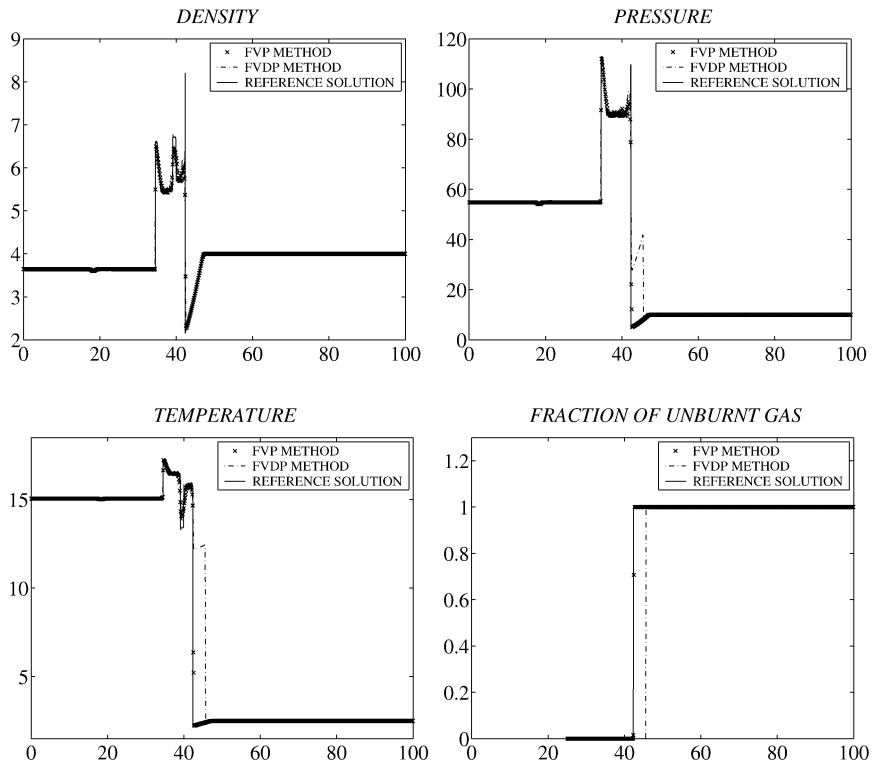


Fig. 11. Solutions of (4)–(5), (28)–(29) computed by both the FVP and FVDP methods at  $t = 4$ .

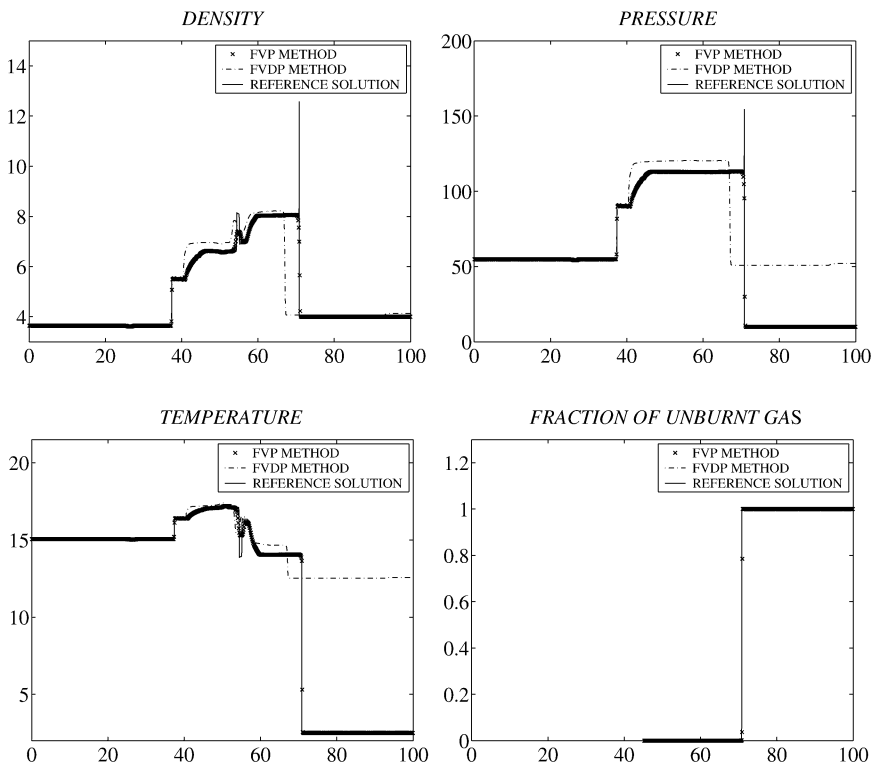


Fig. 12. Solutions of (4)–(5), (28)–(29) computed by both the FVP and FVDP methods at  $t = 8$ .

discontinuities, obtained by the FVP method, are correct. Finally, in Fig. 12, we present the results obtained at time  $t = 8$  (after all the collisions). The computations by the FVDP method are now completely wrong, while the resolution, achieved by the FVP method, is as high as at the smaller times.

## Acknowledgement

The work of A. Chertock was supported in part by the NSF Grant # DMS-0410023. The research of A. Kurganov was supported in part by the NSF Grant # DMS-0310585.

## References

- [1] W. Bao, S. Jin, The random projection method for hyperbolic conservation laws with stiff reaction terms, *J. Comput. Phys.* 163 (2000) 216–248.
- [2] W. Bao, S. Jin, The random projection method for stiff detonation capturing, *SIAM J. Sci. Comput.* 23 (2001) 1000–1026.
- [3] M. Ben-Artzi, The generalized Riemann problem for reactive flows, *J. Comput. Phys.* 81 (1989) 70–101.
- [4] F. Bouchut, F. James, One-dimensional transport equations with discontinuous coefficients, *Nonlinear Anal.* 32 (1998) 891–933.
- [5] F. Bouchut, F. James, S. Mancini, Uniqueness and weak stability for multi-dimensional transport equations with one-sided Lipschitz coefficients, *Ann. Scuola Norm. Sup. Pisa Cl. Sci. (5) IV* (2005) 1–25.
- [6] I. Capuzzo-Dolcetta, B. Perthame, On some analogy between different approaches to first order PDE's with nonsmooth coefficients, *Adv. Math. Sci. Appl.* (1996) 689–703.
- [7] A. Chertock, A. Kurganov, On a hybrid finite-volume-particle method, *M2AN Math. Model. Numer. Anal.* 38 (2004) 1071–1091.
- [8] A. Chertock, A. Kurganov, G. Petrova, Finite-volume-particle methods for models of transport of pollutant in shallow water, *J. Sci. Comput.*, in press.
- [9] A. Cohen, B. Perthame, Optimal approximations of transport equations by particle and pseudoparticle methods, *SIAM J. Math. Anal.* 32 (2000) 616–636.
- [10] P. Collela, A. Majda, V. Roytburd, Theoretical and numerical structure for reactive shock waves, *SIAM J. Sci. Statist. Comput.* 7 (1986) 1059–1080.
- [11] E. Conway, Generalized solutions of linear differential equations with discontinuous coefficients and the uniqueness question for multidimensional quasilinear conservation laws, *J. Math. Anal. Appl.* 18 (1967) 238–251.
- [12] G.-H. Cottet, P.D. Koumoutsakos, *Vortex Methods*, Cambridge University Press, Cambridge, 2000.
- [13] R. Courant, K.O. Friedrichs, *Supersonic Flow and Shock Waves*, Applied Mathematical Sciences, vol. 21, Springer, New York, 1976. Reprinting of the 1948 original.
- [14] D.R. Durran, *Numerical Methods for Wave Equations in Geophysical Fluid Dynamics*, Springer, New York, 1999.
- [15] B. Engquist, P. Lötstedt, B. Sjögreen, Nonlinear filters for efficient shock computation, *Math. Comp.* 52 (1989) 509–537.
- [16] A.F. Filippov, Differential equations with discontinuous right-hand side, *Mat. Sb. (N.S.)* 51 (93) (1960) 99–231 (in Russian).
- [17] A.F. Filippov, Differential equations with discontinuous right-hand side, *Amer. Math. Soc. Transl.* 42 (1964) 199–231.
- [18] A.F. Filippov, *Differential Equations with Discontinuous Right-Hand Side*, Mathematics and its Applications (Soviet Series), vol. 18, Kluwer Academic, Dordrecht, 1988.
- [19] R.T. Glassey, *The Cauchy Problem in Kinetic Theory*, SIAM, Philadelphia, PA, 1996.
- [20] E. Godlewski, P.-A. Raviart, *Numerical Approximation of Hyperbolic Systems of Conservation Laws*, Springer, New York, 1996.
- [21] L. Gosse, F. James, Numerical approximations of one-dimensional linear conservation equations with discontinuous coefficients, *Math. Comp.* 69 (2000) 987–1015.
- [22] S. Gottlieb, C.-W. Shu, E. Tadmor, High order time discretization methods with the strong stability property, *SIAM Rev.* 43 (2001) 89–112.
- [23] F.H. Harlow, *The Particle-in-Cell Method for Fluid Dynamics*, Methods in Computational Physics, vol. 3, Academic Press, New York, 1964.
- [24] C. Helzel, R.J. LeVeque, G. Warnecke, A modified fractional step method for the accurate approximation of detonation waves, *SIAM J. Sci. Comput.* 22 (2000) 1489–1510.
- [25] P. Hwang, R.P. Fedkiw, B. Merriman, T.D. Aslam, A.R. Karagozian, S.J. Osher, Numerical resolution of pulsating detonation waves, *Combust. Theory Modelling* 4 (2000) 217–240.
- [26] D. Kröner, *Numerical Schemes for Conservation Laws*, Wiley, Chichester, 1997.
- [27] A. Kurganov, An accurate deterministic projection method for hyperbolic system with stiff source term, in: T.Y. Hou, E. Tadmor (Eds.), *Hyperbolic Problems: Theory, Numerics, Applications*, Springer, Berlin, 2003, pp. 665–674.
- [28] A. Kurganov, C.-T. Lin, On the reduction of numerical dissipation in central-upwind schemes, *Commun. Comput. Phys.*, submitted for publication.
- [29] A. Kurganov, S. Noelle, G. Petrova, Semi-discrete central-upwind schemes for hyperbolic conservation laws and Hamilton–Jacobi equations, *SIAM J. Sci. Comput.* 21 (2001) 707–740.
- [30] A. Kurganov, E. Tadmor, New high-resolution central schemes for nonlinear conservation laws and convection–diffusion equations, *J. Comput. Phys.* 160 (2000) 241–282.
- [31] B. van Leer, Towards the ultimate conservative difference scheme, V. A second order sequel to Godunov's method, *J. Comput. Phys.* 32 (1979) 101–136.
- [32] A. Leonard, Vortex methods for flow simulation, *J. Comput. Phys.* 37 (1980) 289–335.

- [33] A. Leonard, Computing three-dimensional incompressible flows with vortex elements, *Annu. Rev. Fluid Mech.* 17 (1985) 523–559.
- [34] R.J. LeVeque, High-resolution conservative algorithms for advection in incompressible flow, *SIAM J. Numer. Anal.* 33 (1996) 627–665.
- [35] A.A. Medovikov, High order explicit methods for parabolic equations, *BIT* 38 (1998) 372–390.
- [36] A.A. Medovikov, DUMKA3 code, <http://www.math.tulane.edu/~amedovik>.
- [37] R.J. LeVeque, *Finite Volume Methods for Hyperbolic Problems*, Cambridge Texts in Applied Mathematics, Cambridge University Press, Cambridge, 2002.
- [38] R.J. LeVeque, H.C. Yee, A study of numerical methods for hyperbolic conservation laws with stiff source terms, *J. Comput. Phys.* 86 (1990) 187–210.
- [39] H. Nessyahu, E. Tadmor, Non-oscillatory central differencing for hyperbolic conservation laws, *J. Comput. Phys.* 87 (1990) 408–463.
- [40] F. Poupaud, M. Rascle, Measure solutions to the linear multi-dimensional transport equation with non-smooth coefficients, *Comm. Partial Differential Equations* 22 (1997) 337–358.
- [41] P.A. Raviart, An analysis of particle methods, in: *Numerical Methods in Fluid Dynamics*, Como, 1983, Lecture Notes in Math., vol. 1127, Springer, Berlin, 1985, pp. 243–324.
- [42] P.K. Sweby, High resolution schemes using flux limiters for hyperbolic conservation laws, *SIAM J. Numer. Anal.* 21 (1984) 995–1011.
- [43] E. Tadmor, Local error estimates for discontinuous solutions of nonlinear hyperbolic equations, *SIAM J. Numer. Anal.* 28 (1991) 891–906.